

Dynamics of Molecules near Ionization

Theis I. Sølling,[†] Carsten Kötting,[‡] and Ahmed H. Zewail*

Arthur Amos Noyes Laboratory of Chemical Physics, California Institute of Technology, Pasadena, California 91125

Received: June 30, 2003; In Final Form: September 22, 2003

In this paper, we report our experimental studies, using femtosecond-resolved mass spectrometry, and theoretical calculations of the potential energy surfaces, using density functional theory, for 10 aliphatic amines (substituted ammonia) excited directly near the ionization continuum. By probing parent and fragment masses, we are able to decipher pathways of the reactive α -cleavage and the nonreactive internal conversion, a precursor for the following chemistry. The bifurcation in these channels is related to the structure, as evidenced by the dramatic effect of α -substitution vs *N*-substitution on the time scale of the dynamics—femtosecond vs picosecond rates. For all molecules studied, the observed branching is dependent on the change of character of the state, ionic and/or neutral, along the reaction coordinate, and this change blurs the distinction between Rydberg and Superexcited states in their subsequent reactivity.

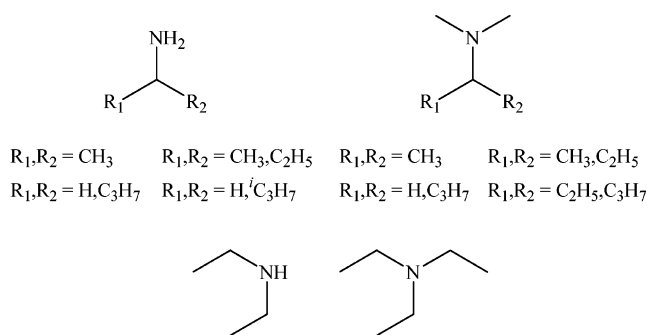
Introduction

Molecules near ionization have bound or quasi-bound states. Below ionization, they are the well-known Rydberg states. The so-called superexcited states are defined as the electronically excited states with an excitation energy above the lowest ionization threshold.^{1,2} Both states play an important role in the chemistry of large molecules excited at high energies. For example, in this laboratory, femtochemistry studies of ketones,^{3,4} alkyl halides,⁵ and others^{6,7} involve these high-energy Rydberg states as a doorway to many reactions.

Superexcited states have been prepared under a variety of experimental conditions.^{8–10} For example, their direct relevance was shown in a recent femtosecond-resolved photoelectron spectroscopy study of phenol and 1,3-cyclohexadiene.⁸ In general, ionization is an exothermic process for superexcited species, with the possibility of autoionization, but the formation of ions (and ejection of an electron) is not always on the ultrafast time scale. It has been reported that superexcited species, in some cases, can be very long-lived, up to microseconds.^{9b} The role of these states has been examined in the decomposition of ionized (by electron impact) amines,^{1,2,10} and also in a series of neutral amines.^{2,10}

The nuclear motions involved in bond breaking reactions can only be studied on the femtosecond time scale.⁶ The homolytic cleavage of a single C–C σ -bond is a common photochemical reaction of organic molecules in the condensed as well as in the gas phase.¹¹ The Norrish type-I reaction of ketones is a well-known example of this C–C bond rupture whose femtosecond reaction dynamics involves, besides the rupturing C–C bond, a subset of nuclear motions, defining the reaction coordinate to include not only the C–C stretch.³ Such C–C bond ruptures, referred to as simple cleavages, have also been studied for ionized amines and have been found to be more complicated

CHART 1: Two Classes of Amines Studied



than they appear to be.^{12–14} To elucidate the reactive and nonreactive pathways of these near-ionization excitations, we present here femtosecond-resolved time-of-flight mass spectrometric (FS-TOF) studies of aliphatic amines. Unlike ketones, they do not have low-energy valence states and we can reach their superexcited states through high-energy multiphoton (with no intermediate) excitations. All these amines have in common the “ammonia-type” moiety and we studied 10 of them (Chart 1).

The systems under study were chosen to represent vertical ionization potentials that are higher as well as lower than our excitation energy (186 kcal mol⁻¹). Conveniently, the vertical ionization potential varies with alkyl substitution on the nitrogen; alkyl groups stabilize the radical cation and hence reduce the vertical ionization potential. The systems studied, shown and named in Figure 1, represent different classes of substitution around the nitrogen and carbon atoms.

For radical cations of aliphatic amines formed by electron-impact ionization the detailed mechanism of α -cleavage has been discussed.^{12–14} It has also been shown¹⁵ that simple cleavage is the predominant reaction in their radical cations formed by multiphoton ionization and that the yield of fragment ions is independent of the laser intensity but highly dependent on the employed wavelength. For neutral amines the picture is less clear. The first excited state in amines is reached by an

* To whom correspondence should be addressed. Fax: +1 626 792 8456. E-mail: zewail@caltech.edu.

[†] Current address: Danish Polymer Center, Risø National Laboratory, Frederiksborgvej 399, DK-4000 Roskilde, Denmark.

[‡] Current address: Lehrstuhl für Biophysik, ND 04/352, Ruhr-Universität Bochum, D-44780 Bochum, Germany.

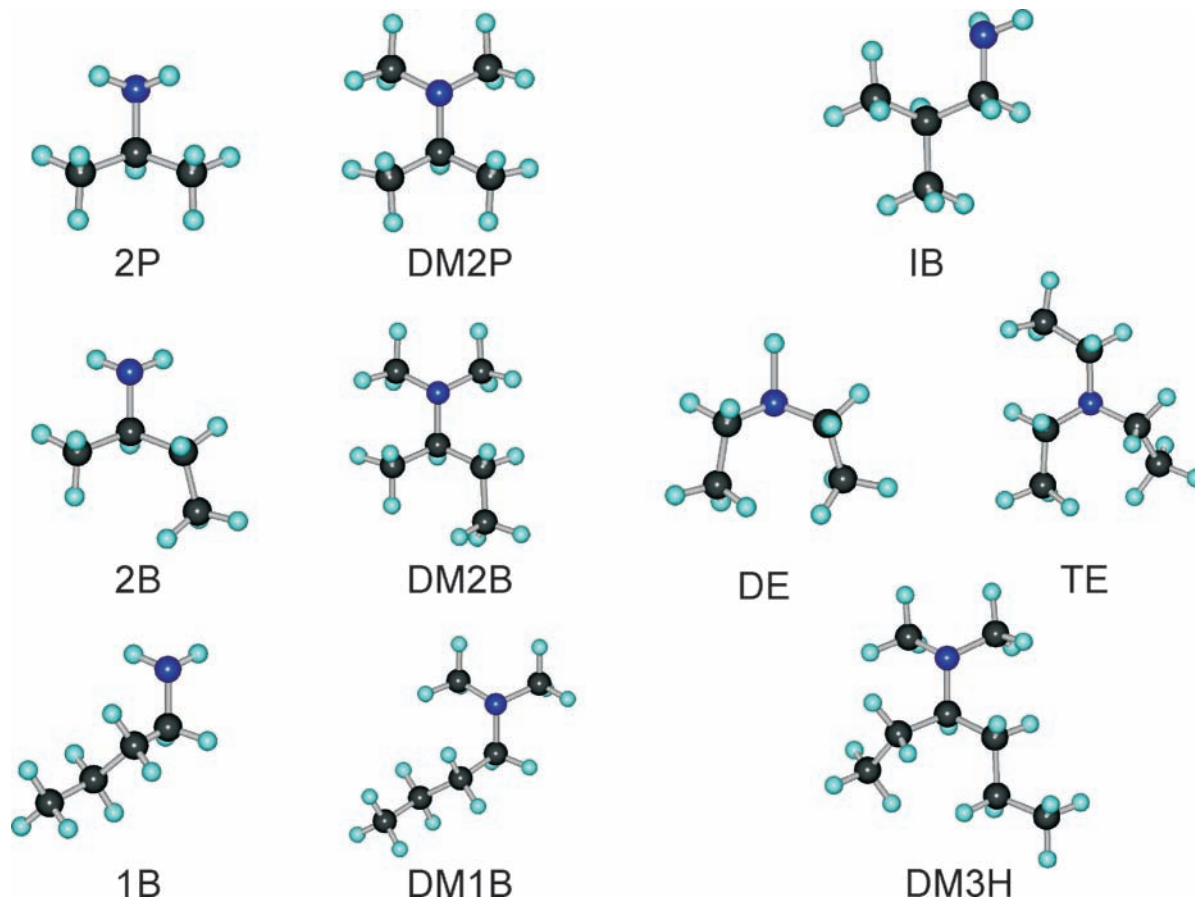


Figure 1. Aliphatic amines under study.

$n \rightarrow 3s$ Rydberg transition, as addressed in ref 16 and by other studies (see refs 17–21); the vast majority of accessible excited states in aliphatic amines are Rydberg states,^{19–21} with rather narrow absorption bands that are indicative of long-lived states.²¹ If broad bands were found, it was argued that dissociation occurs. In addition to the C–C rupture, C–N cleavage has been mentioned as have the losses of atomic and molecular hydrogen.^{17,18}

This contribution gives our experimental and theoretical studies of the reaction dynamics of aliphatic amines near ionization on the femtosecond time scale and presents a description of nuclear motions involved in the reactive and nonreactive channels. The paper is organized as follows. In the Experimental Section and Computational Methods, the experimental apparatus, measurement techniques, and theoretical procedures are described, and this is followed by the Results and Discussion; the first part of this section details the experimental results for the ion chemistry and the time-resolved studies, whereas the second part describes our theoretical studies and gives a discussion of the dynamics. Experiment and theory are combined in the final section to provide a concluding general picture of the reactive and nonreactive pathways of aliphatic amines near ionization.

Experimental Section

The femtosecond (fs) laser and molecular beam apparatus have been described in detail elsewhere.^{22,23} Briefly, the output of a colliding-pulse, mode-locked oscillator (CPM) was amplified with a four-stage dye amplifier, pumped by a Nd:YAG laser at 20 Hz. The output, after recompression by a four prism setup, was typically an 80 fs wide (Gaussian) pulse with an intensity of $\sim 150 \mu\text{J}/\text{pulse}$ at 615 nm. It was split to provide

the pump pulse for excitation and the probe pulse for ionization; for the pump, the 615 nm output was frequency doubled whereas it was passed directly to a computer-controlled translation stage for the time delay and was used as probe in that manner. The time zero was measured in situ using xenon as a reference.²⁴

The pump and probe pulses were spatially combined and were focused into the supersonic molecular beam apparatus containing the time-of-flight mass spectrometer. Both pump and probe pulses were appropriately attenuated to minimize background signals and the intensities of the pump and probe pulses were chosen such that the absorption of two pump photons is the most likely process observed. In fact, the available absorption spectra of aliphatic amines indicate that a state does not exist to match a single 307 nm photon. By gating the signal due to ions with a particular mass, the temporal evolution of each species was measured.

The compounds under study were obtained from Aldrich and used without further purification; the mass spectra reflect the purity. Some were prepared (DM3H and DM2B) by standard synthesis procedures. The samples were seeded in a He carrier gas at a total stagnation pressure of 2 bar. The pressure within the molecular beam apparatus was maintained at 5×10^{-6} Torr. The nozzle temperature was kept at ~ 100 °C to prevent clustering.

Computational Methods

The energetics for the involved ionic species were calculated using density functional theory at the B3LYP/6-31G(d) level in the case of reactions on the ground-state surfaces. The zero point vibrational energies were scaled by 1.008 as suggested by Scott and Radom.²⁵ In the case of excited-state species, the energetics were calculated using the TD-B3LYP/6-31++G(2df)

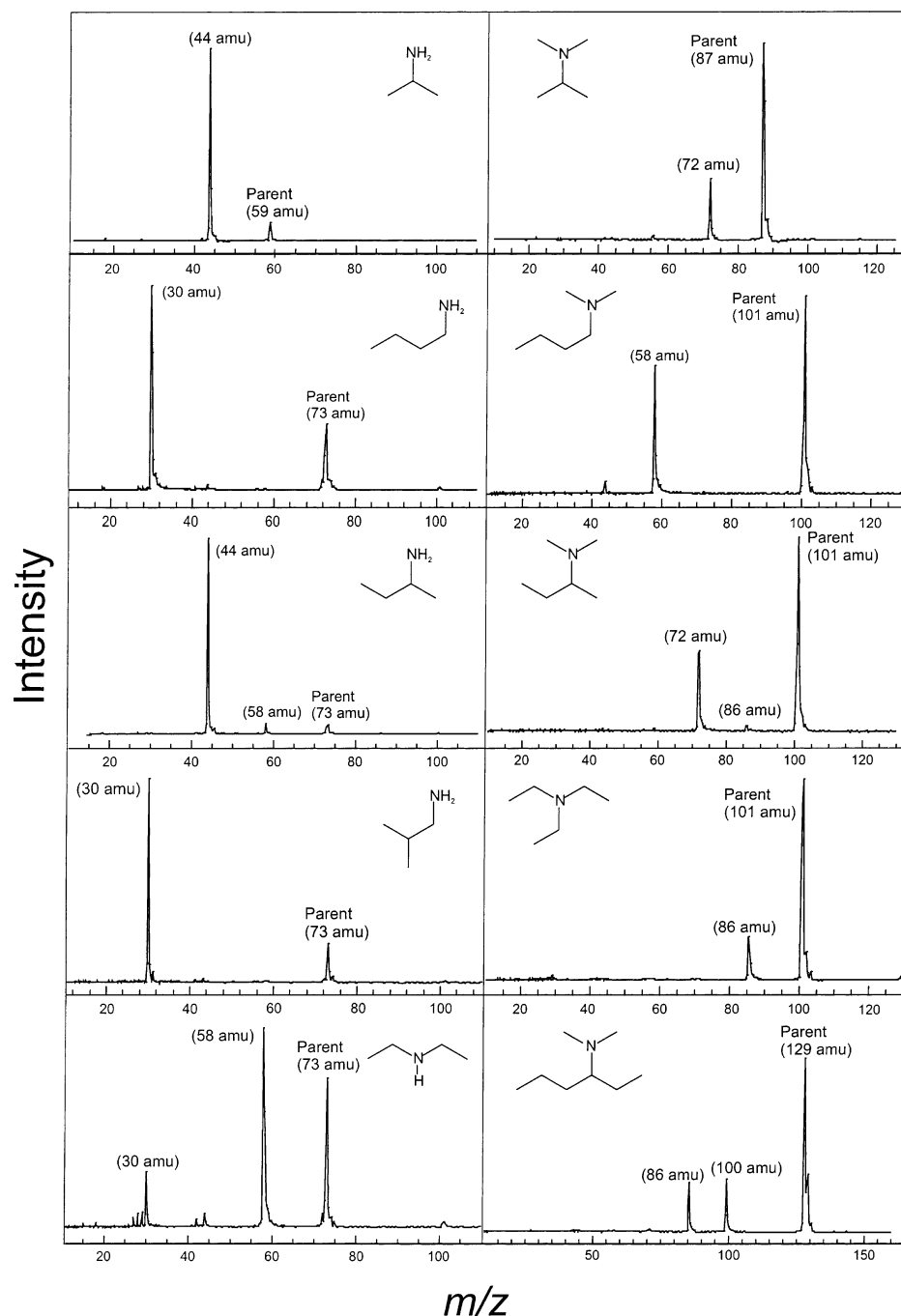


Figure 2. Femtosecond multiphoton ionization mass spectra of aliphatic amines recorded at a time delay of less than 50 fs.

level on B3LYP/6-31+G(d) optimized geometries, unless stated otherwise. The 6-31++G(2df) basis set was chosen because it was found that the agreement with the experimental excitation energy²¹ for the $n \rightarrow 3s$ Rydberg excitation in gaseous isopropylamine (2P) is satisfactory. This amine and its dimethylated (DM2P) counterpart are chosen as prototypical systems in the computational part of this study. The scan along the nitrogen inversion coordinate was qualitatively similar to that obtained at the TD-B3LYP/6-31+G(d) level. To reduce the computational cost, this level was employed in the scan along the α -C–C coordinates. The calculations were carried out with the GAUSSIAN 98 program package.²⁶

Results and Discussion

Ion Chemistry. In Figure 2 we display the mass spectra of the investigated amines ionized by femtosecond laser pulses.

The ionized amines spend on the order of 0.1 μ s in the acceleration region of the TOF mass spectrometer and hence this is the time window of the ionic reactions in question. The mass spectra were recorded near zero time delay between the pump and the probe pulses to ensure minimum decomposition of the neutral parent species in the mass spectra. It is the utilization of femtosecond pulses that enables the selective ionization of the parent and therefore offers the prospect of observing the ion chemistry of the parent species in question. With the exception of diethylamine (DE) the only decomposition channel of the amine radical cations is loss of an alkyl radical to form an immonium ion:

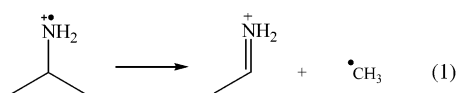
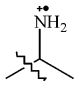
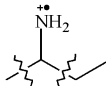
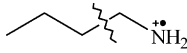
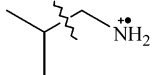
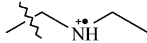
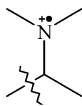
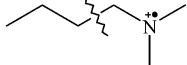
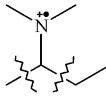
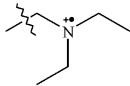
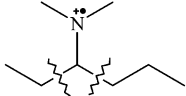


TABLE 1: Reaction Energies for C–C Bond Breakage in Ionized Amines and the Vertical and Adiabatic Ionization Energies of the Corresponding Neutral Molecule^a

Molecule	$\Delta_r H$	Vertical IE	Adiabatic IE
	0.51	9.10	8.30
	0.54/0.53 ^b	9.04	8.13
	1.21	9.13	8.16
	1.10	9.07	8.17
	1.26	8.47	7.72
	0.86	8.00	7.25
	1.37	8.00	7.19
	0.91/0.84 ^b	7.70	7.01
	1.31	7.82	7.08
	0.81/0.84 ^b	7.44	6.90

^a 0 K, B3LYP/6-31G(d), values in eV. ^b Loss of the larger alkyl fragment.

In the case of DE the immonium ion that is formed by the initial bond breakage further fragments. The literature 70 eV mass spectrum shows that this is also the case when the ionization is induced by electron impact.²⁷

The mass spectra of the asymmetric amine radical cations (2B, DM2B, and DM3H) show that the competition between loss of the larger and the smaller alkyl radical favors loss of the larger alkyl radical in the case of 2B and DM2B and the smaller one in the case of DM3H, which in all cases means that an ethyl radical is lost most readily. The calculated reaction energies for the decompositions of the amine radical cations are shown in Table 1. It can be seen that the fragmentation pattern is in line with the calculated reaction energies; i.e., the energetically preferred reaction is ethyl loss from 2B, DM2B and DM3H. This behavior is opposite to that of aliphatic ketones^{3d} under the same experimental conditions and to that of aliphatic amines that have been subjected to 70 eV electron-impact ionization. In these systems the reaction with the higher energy demand surprisingly proceeds in a higher

yield.^{14,28} This illustrates that the competition between the loss of alkyl fragments from asymmetric cation radicals is determined by an interplay between the relative barrier heights and the available internal energy, as discussed previously.^{3d,14}

Femtosecond-Resolved Mass Spectra and Effect of Structure. The temporal evolution of the parent and fragment ion currents has been recorded to shed light on the dynamical features that result when the neutral species absorb two 307 nm photons. For the systems discussed, the dependence of the ion current (S) on the pump intensity (I) confirmed that the pump process involves the absorption of two photons ($186 \text{ kcal mol}^{-1}$). Two representative power dependencies ($\ln(S)$ vs $\ln(I_{\text{pu}})$) are shown in Figure 3 at a 50 fs and longer time delay; one represents amines with IE above $186 \text{ kcal mol}^{-1}$, and the other represents amines with an IE below $186 \text{ kcal mol}^{-1}$. The slope of the straight lines is near, but not exactly, 2. Because there is no intermediate state present, we expect a slope of 2. However, as pointed out in ref 29, the central portion of the laser beam

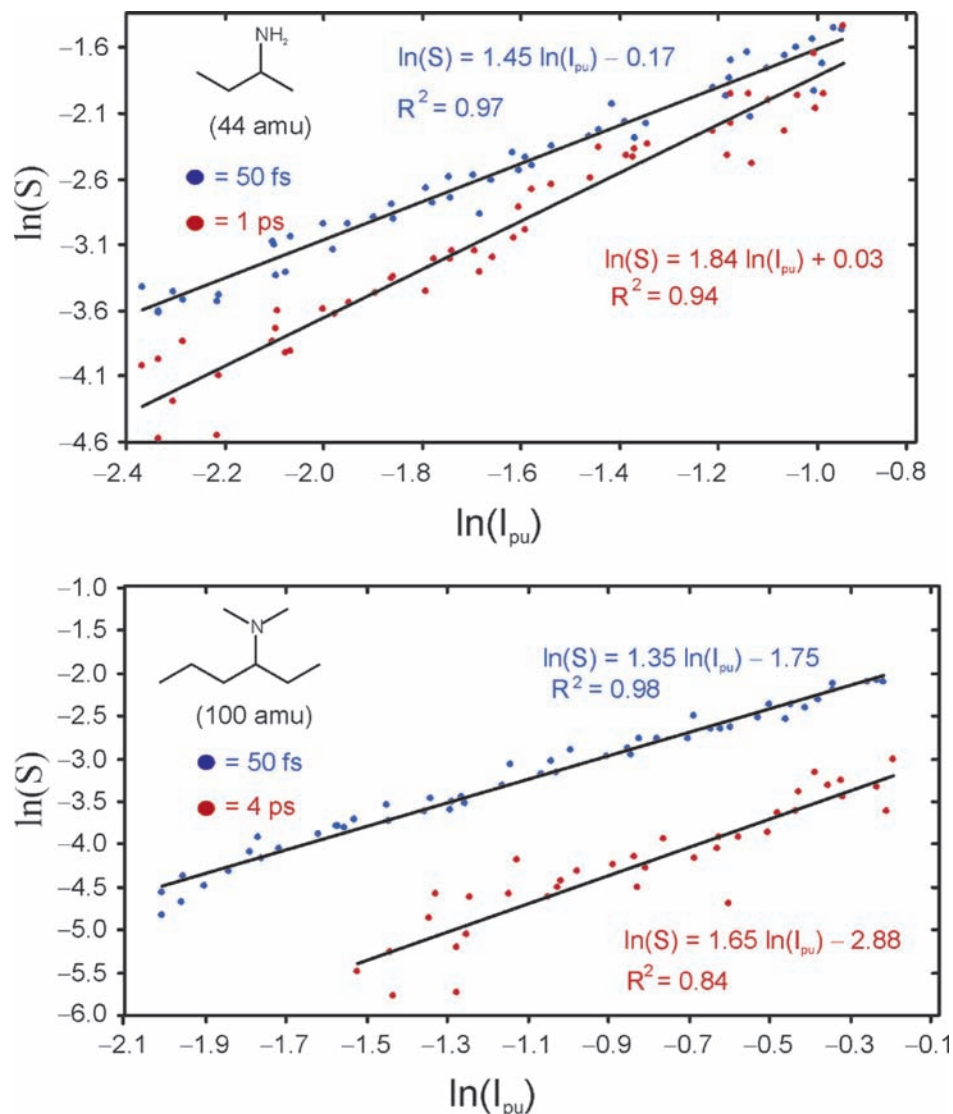


Figure 3. Relation between the pump-laser power (I_{pu}) and ion current (S) for the most abundant fragment ions from 2B and DM3H at short (blue dots) and long (red dots) delay times.

contributes differently from the weaker tails. The femtosecond transients are shown in Figures 4–8.

The transients corresponding to the parent mass can in all but one case (DE, Figure 7) be fitted to a single-exponential decay. In the case of some of the transients taken at a fragment mass a second exponential and a component that accounts for a depletion of the signal at positive times are required to obtain a good fit. The kinetics equation is shown in eq 2, and the elementary steps follow those of α -cleavage in ketones, where as in ref 3d, A and B refer to the states of the parent and C is that of the product radical:



The solution of these equations is straightforward³⁰ but we must include the response function.³¹ In contrast to the case for ketones, where the acyl radical decomposes further, the product radical in the present case is stable and there is no need for an additional time constant to be included. The time constants obtained from the transients are given in Table 2. The most striking feature of the transients in Figures 4–8 is the dramatic effect of alkyl substitution of the nitrogen atom. The substitution of two methyl groups on the nitrogen atom introduces a picosecond component; i.e., the derived time constants increase

by up to a factor 30. It can be seen from Table 2 that the decay times that are associated with the picosecond components (τ_1) increase as the size of the amine increases. On the other hand, the time constants that are derived from the transients taken at the parent mass (τ_0) are longer when a primary amine is compared with its dimethylated counterpart.

Figure 6 shows the transients for the asymmetrical amines 2B, DM2B, and DM3H recorded at the parent mass (e.g., $\text{CH}_3\text{CH}(\text{NH}_2)\text{CH}_2\text{CH}_3^+$) and at the fragment masses (e.g., $\text{CH}_3\text{CH}=\text{NH}_2^+$). The asymmetric amines give rise to two different fragment ions and the time constants (τ_1) that can be obtained from either of the fragment transients are the same. If these time constants reflect processes involving the corresponding neutrals (e.g., $\text{CH}_3\dot{\text{C}}\text{HNH}_2$ and $\text{CH}_3\text{CH}_2\dot{\text{C}}\text{HNH}_2$ from 2B) transients taken at two different fragment masses should give rise to different time constants, because the neutrals are chemically distinct species. The fact that this is not the case for any of the three investigated asymmetric amines indicates that the fragment ions are formed by decomposition of the ionized parent species in the acceleration region of the time-of-flight mass spectrometer and not by direct ionization of a neutral amino alkyl radical.

The result that no picosecond component is observed in the transients, taken at the parent masses, suggests that the

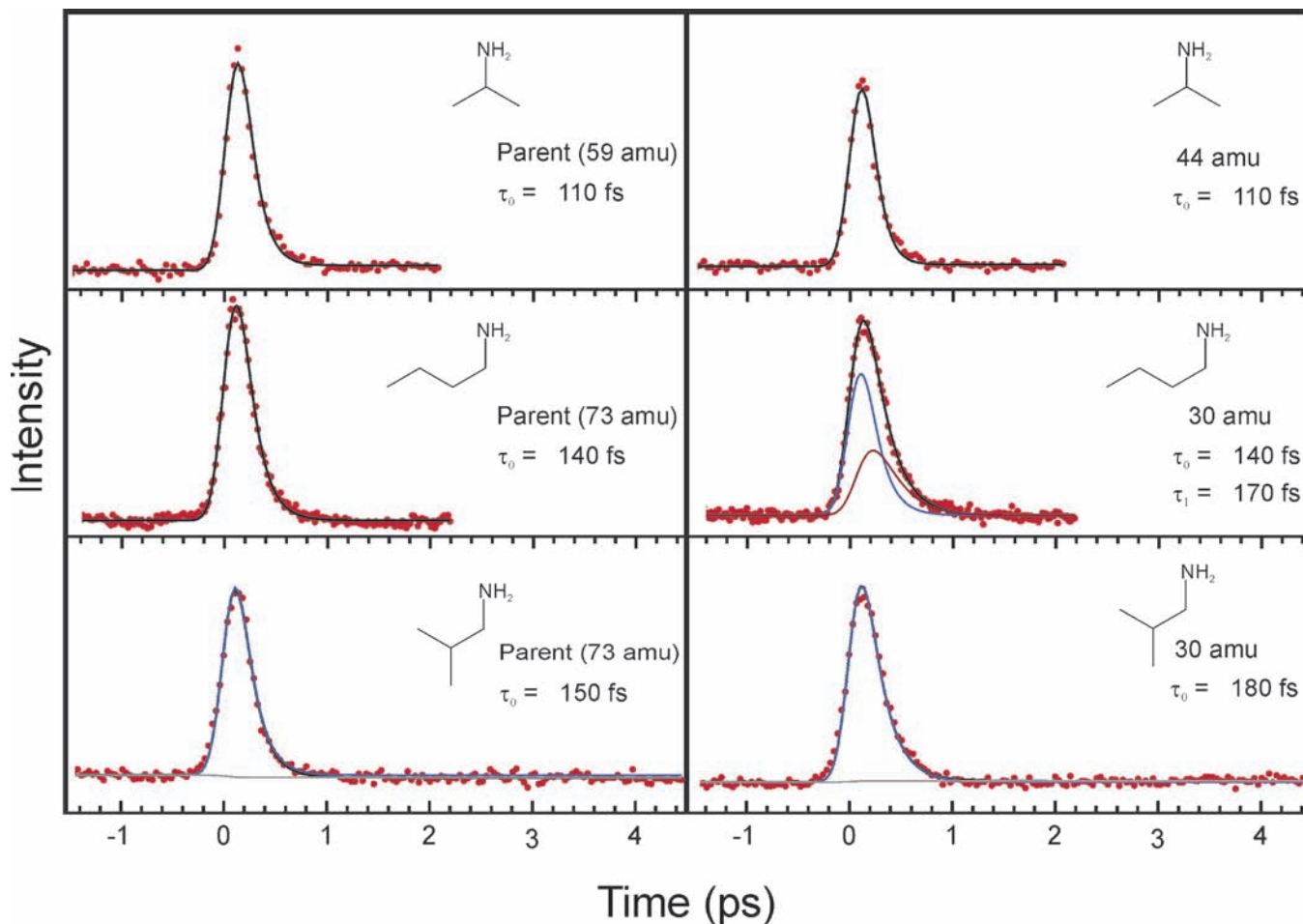


Figure 4. Time-resolved ion currents of primary amines. The results for the parent ions are shown to the left whereas the results for the fragment ions are shown to the right. The experimental data points are given as red dots, and the overall fit is shown in black. The components of the transients are represented by different colors. The blue curve corresponds to the initial processes with the decay time of τ_0 in the parent. The bordeaux line represents (when required) the component that rises with τ_0 and decays with τ_1 . The gray line is the component that describes the offset or the depletion.

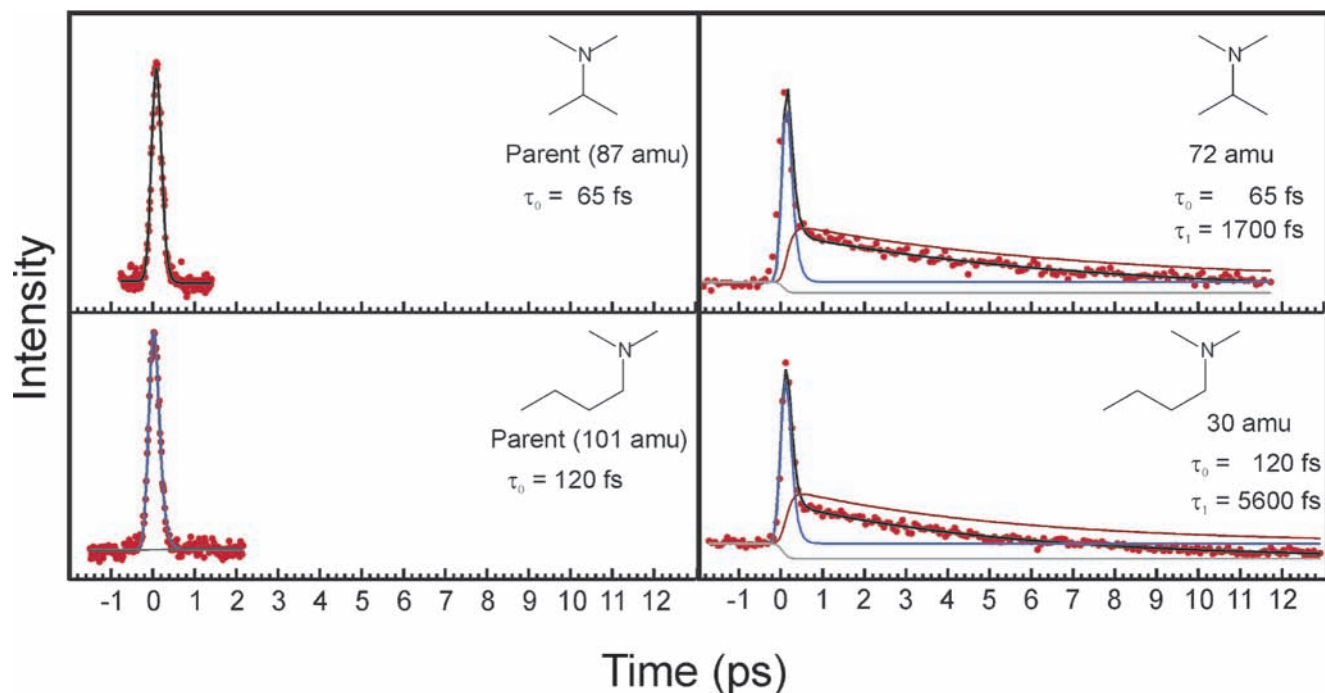


Figure 5. Time-resolved ion currents of tertiary amines (the dimethylated counterparts of the amines in Figure 4). The results for the parent ions are shown to the left whereas the results for the fragment ions are shown to the right. The experimental data points are given as red dots and the overall fit is shown in black. The components of the transients are represented by different colors; color coding is the same as in Figure 4.

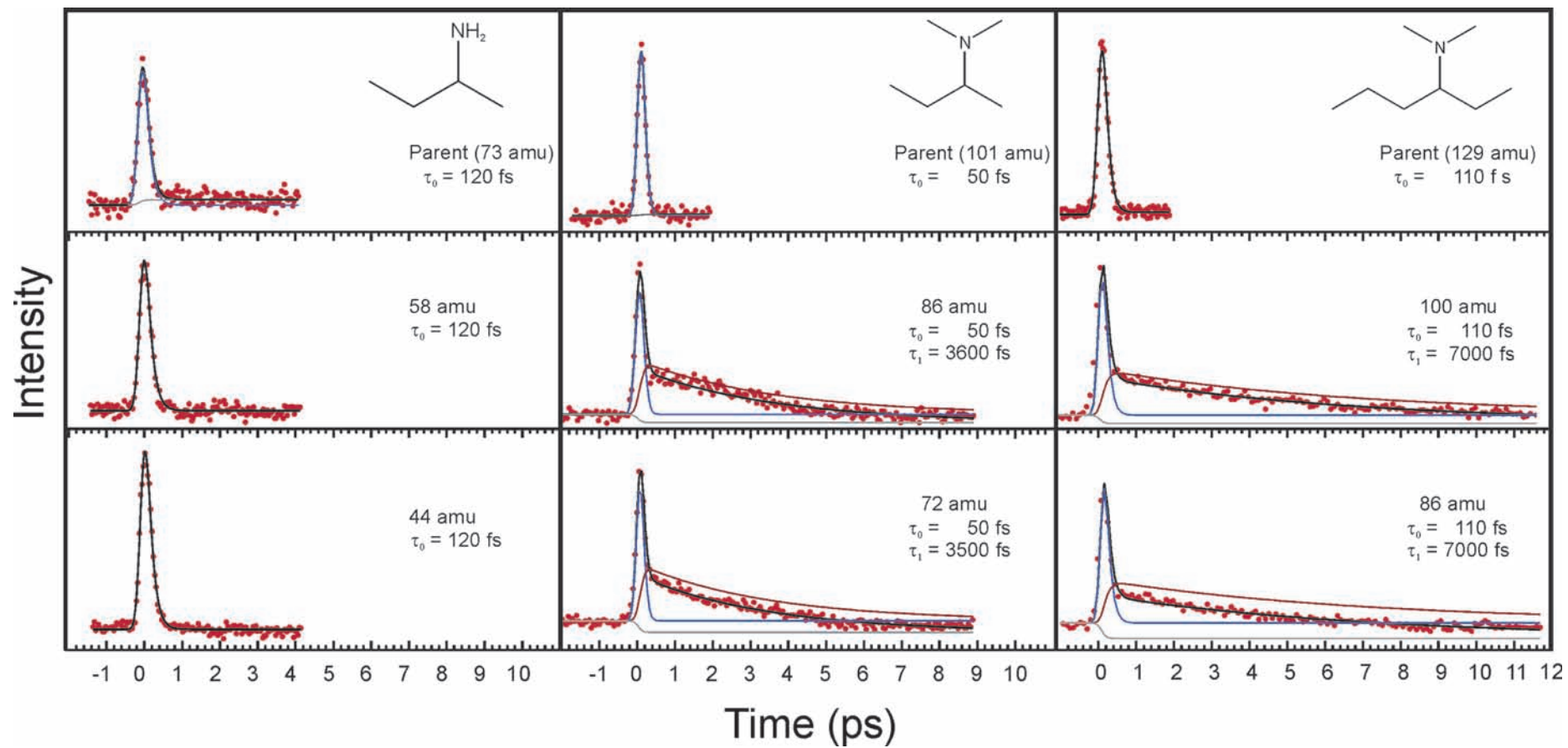
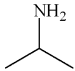
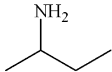
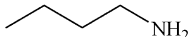
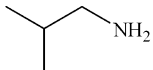
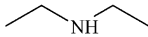
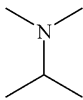
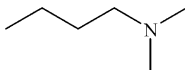
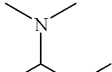
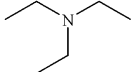
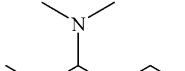


Figure 6. Time-resolved ion currents of primary and tertiary amines with two different α -alkyl groups. The experimental data points are given as red dots and the overall fit is shown in black. The components of the transients are represented by different colors; color coding is the same as in Figure 4.

TABLE 2: Time Constants Related to the Photophysical and Photochemical Processes of Aliphatic Amines (fs)^a

Molecule	Probed Species		τ_0^a	τ_1^a
	Parent	(<i>m/z</i> 59)	110	
	CH ₃ CH=NH ₂ ⁺	(<i>m/z</i> 44)	110	
	Parent	(<i>m/z</i> 73)	120	
	CH ₃ CH ₂ CH=NH ₂ ⁺	(<i>m/z</i> 58)	120	
	CH ₃ CH=NH ₂ ⁺	(<i>m/z</i> 44)	120	
	Parent	(<i>m/z</i> 73)	140	
	CH ₂ =NH ₂ ⁺	(<i>m/z</i> 30)	140	
			170	
	Parent	(<i>m/z</i> 73)	150	
	CH ₂ =NH ₂ ⁺	(<i>m/z</i> 30)	180	
	Parent	(<i>m/z</i> 73)	60	400
	CH ₃ CH ₂ NH=CH ₂ ⁺	(<i>m/z</i> 58)	60	400
	Parent	(<i>m/z</i> 87)	65	
	CH ₃ CH=N(CH ₃) ₂ ⁺	(<i>m/z</i> 72)	65	1700
	Parent	(<i>m/z</i> 101)	120	
	CH ₂ =N(CH ₃) ₂ ⁺	(<i>m/z</i> 58)	120	5600
	Parent	(<i>m/z</i> 101)	50	
	CH ₃ CH ₂ CH=N(CH ₃) ₂ ⁺	(<i>m/z</i> 86)	50	3600
	CH ₃ CH=N(CH ₃) ₂ ⁺	(<i>m/z</i> 72)	50	3500
	Parent	(<i>m/z</i> 101)	80	
	CH ₃ CH ₂ N(CH ₂ CH ₃)=CH ₂ ⁺	(<i>m/z</i> 86)	80	5700
	Parent	(<i>m/z</i> 129)	110	
	CH ₃ CH ₂ CH ₂ CH=N(CH ₃) ₂ ⁺	(<i>m/z</i> 100)	110	7000
	CH ₃ CH ₂ CH=N(CH ₃) ₂ ⁺	(<i>m/z</i> 86)	110	7000

^a The values are derived from the transients shown in Figures 4–8.

decomposition of the parent ions is complete—at least within the limit of the signal-to-noise ratio of the transients. The reaction energies for the decomposition of the ionized amines are consistent with that idea. They all lie significantly below the combined energy of two pump photons and *one* probe photon (~10 eV). The sum of the numbers in columns 1 and 3 of Table 1 gives the reaction energy for the decomposition relative to the ground state of the neutral. The excess energy (2 eV) that results from the absorption of *one* probe photon would suffice to give virtually complete decomposition in the ~0.1 μs the parent ions spend in the acceleration region of our time-of-flight mass spectrometer. Moreover, it is most likely that the probing process involves the absorption of more than *one* probe photon, giving rise to an even higher excess energy of the parent ion.

Only one secondary amine (DE) has been included in this study, primarily to test whether substitution by a single alkyl group will also give rise to a picosecond component in the transients taken at the fragment masses. It can be seen from Figure 7 that this is not the case. However, there is another

interesting observation to be made. DE is the only case where the parent transient cannot be fitted as a single exponential decay; an additional exponential function is required. The amplitude of this additional component comprises less than 10 % of the parent transient. The transient taken at the fragment mass can be fitted to the same two exponential functions as the parent transient, but the amplitude of the component corresponding to the larger time constant is significantly larger in that case. The behavior of DE is intermediate to that of the primary and the tertiary amines, and the result also points in the direction of decomposition of the ionized (hot) parent ions in the acceleration region of the mass spectrometer. This again indicates that the slower component does not reflect a process in the neutral amino alkyl radical.

The transients shown in Figures 4–8 were obtained using low-intensity probe pulses (~6 μJ pulse⁻¹) to minimize the background signal. More intense probe pulses (~30 μJ pulse⁻¹) change the amplitudes of the various components that are contributing to the transients (Figure 8). It can be seen that the amplitudes of the offset component of the parent transient and

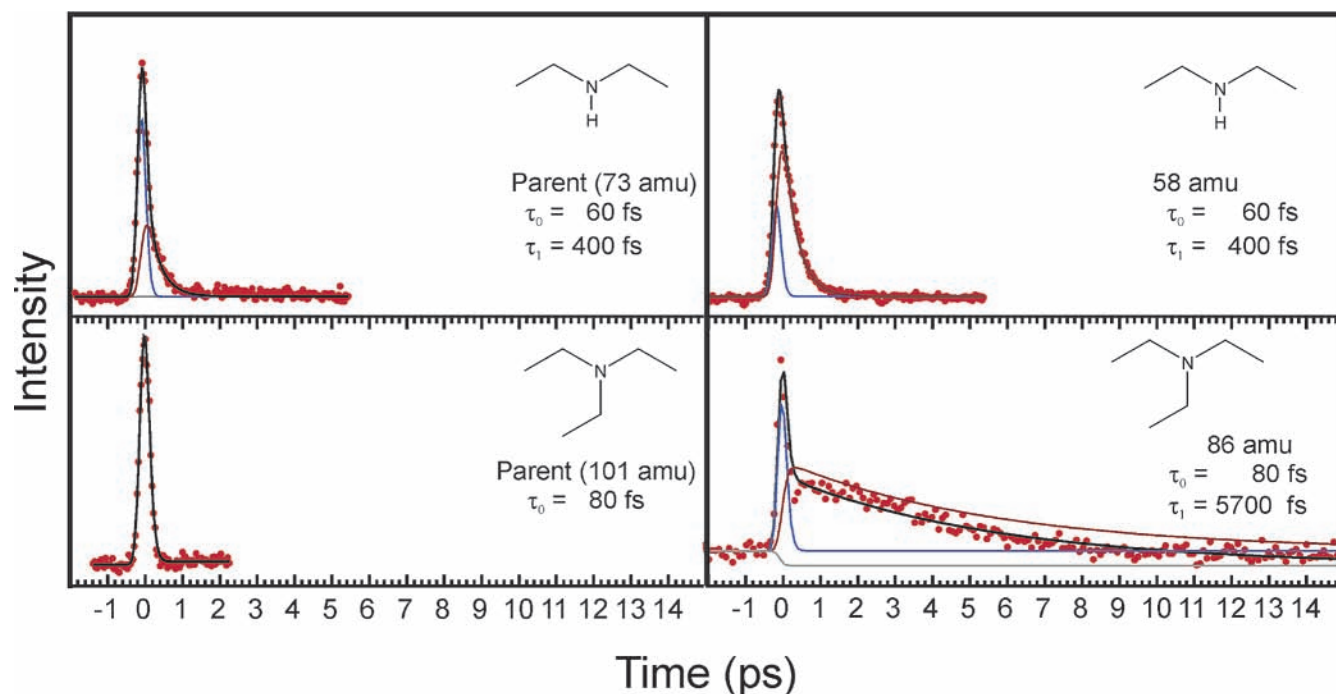


Figure 7. Time-resolved ion currents of diethylamine (DE, a secondary amine) and triethylamine (TE, a tertiary amine). The results for the parent ions are shown to the left whereas the results for the fragment ions are shown to the right. The experimental data points are given as red dots and the overall fit is shown in black. The components of the transients are represented by different colors; color coding is the same as in Figure 4.

TABLE 3: Vertical Excitation Energies of Isopropylamine and *N,N*-Dimethylisopropylamine^a

State	<chem>CC(C)N</chem>	<chem>CC(C)N(C)C</chem>
$A'(n \rightarrow 3s)$	5.32	5.01
$A''(n \rightarrow 3p_y)$	6.20	5.47
$A'(n \rightarrow 3p_z)$	6.21	5.45
$A'(n \rightarrow 3p_x)$	6.36	5.62
$A''(n \rightarrow 3d_{yz})$	6.91	6.23
$A'(n \rightarrow 3d_x^2)$	7.02	6.04

^a TD-B3LYP/6-31++G(2df), values in eV, at 0 K.

the depletion component of the fragment transient increase significantly with the intensity of the probe pulse. By establishing the baseline (i.e., by measuring the ion current with the laser blocked), it was shown in all but one case that the probe pulse does induce enhancement: the ion current induced by the combination of the pump and the probe pulses exceeds the baseline value at positive times. The exception is found for the transient taken at $m/z = 58$ for DE; in this case the apparent depletion is genuine. This indicates further fragmentation of the 58 amu fragment ion. It is in line with this result that the ion current corresponding to the $m/z = 30$ ion from DE again exceeds the background signal.

Theoretical

Absorption Spectra. The vertical absorption energies of 2P and DM2P are given in Table 3. Three points are noteworthy. First, the calculations confirm that there is no state to match the absorption of a single 4 eV pump photon; the lowest lying state is found at 5.01 eV. Second, the excitation energies are

lower in the case of the dimethylated species. Third, there is a state in the vicinity of 6 eV (such a state would be populated by the absorption of three probe photons). The available data for the absorption bands of gaseous amines are limited. For isopropylamine (2P), the absorption maximum corresponding to the $n \rightarrow 3s$ transition lies at 234.75 nm.²¹ The calculated value at the TD-B3LYP/6-31++G(2df) level of theory is 233 nm.

The existence of a state at 6 eV introduces the possibility of a reversal of the pump/probe scheme at negative times; i.e., the 615 nm pulse plays the role of the pump (3 photons) whereas the temporal evolution of the wave packet on the 6 eV state can in principle be monitored by the 307 nm pulse. If the 6 eV wave packet does not evolve on the time scale under consideration the ion current would be higher at negative times (apparent depletion at positive times). At positive times the population is pumped to an 8 eV state; if the probing of this state gives rise to an offset, it will be counterpoised by the offset at negative times. The final result (offset or depletion at positive times) will depend on the experimental conditions (primarily the pulse intensities). We have recently shown that the three 2 eV photon pumping followed by 4 eV probing can contribute significantly to the overall signal at negative times so the result is not surprising.^{5a,b}

The excitation energies in Table 3 all reflect transitions from the nonbonding orbital on nitrogen to a Rydberg orbital. The Rydberg excited species have the character of a cationic core surrounded by a diffuse electron cloud; the nature of such species resembles that of the corresponding radical cation in many respects. Amine radical cations are stabilized more than the neutral by methyl substitution on the nitrogen atom. Accordingly, the excitation energies are lower for the neutral dimethylated amine compared to its unsubstituted counterpart. It has been suggested that there can exist several types of 3s Rydberg states, some which are bonded and some which are not.²⁰ Our TD-DFT calculations show that this is not the case;

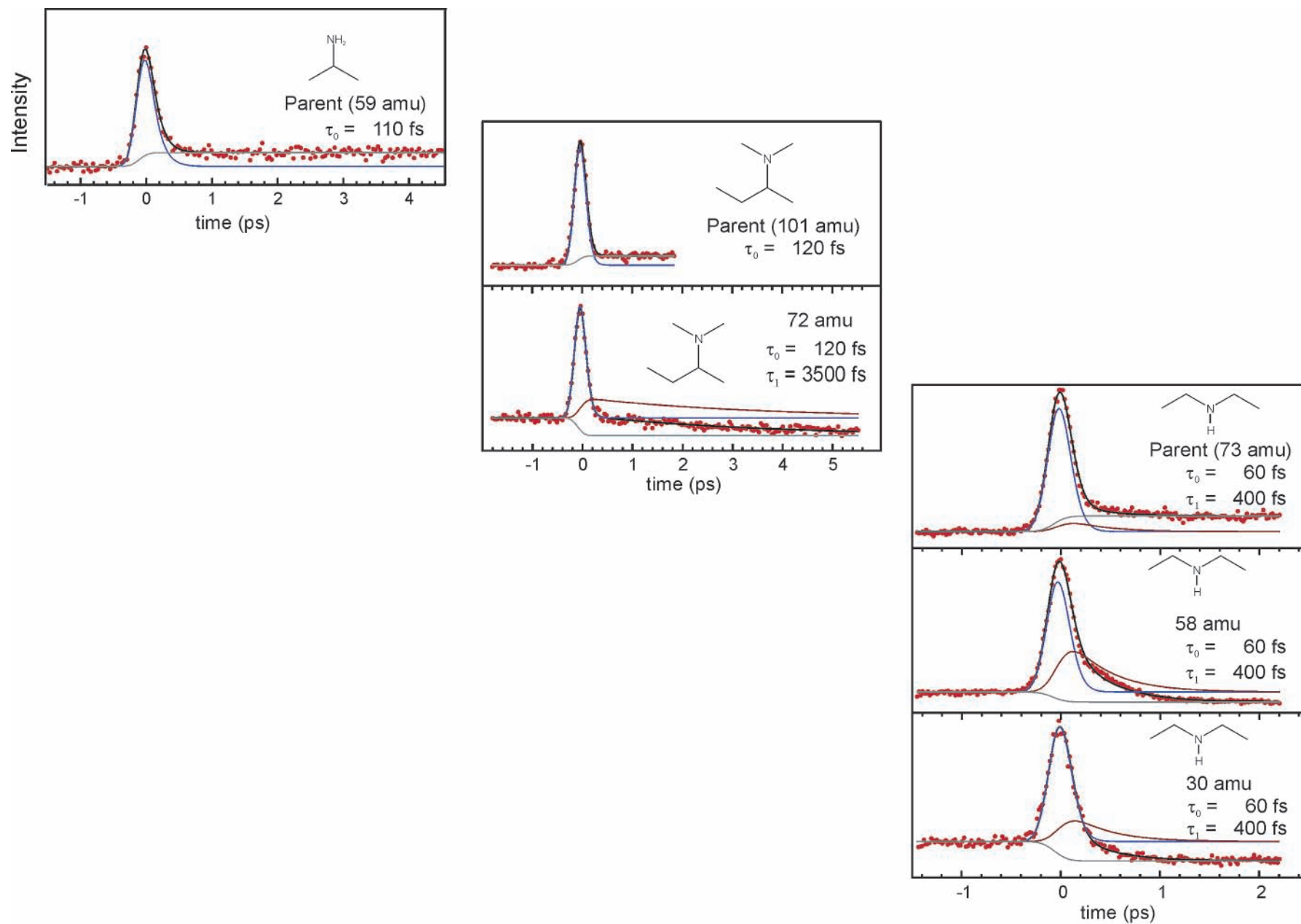


Figure 8. Examples of the effect of high probe power on the time-resolved ion currents that result from primary, secondary, and tertiary amines. Notice the increase in amplitude of the components that correspond to an offset and to depletion (cf. Figures 4, 6, and 7). The experimental data points are given as red dots and the overall fit is shown in black. The components of the transients are represented by different colors; color coding is the same as in Figure 4.

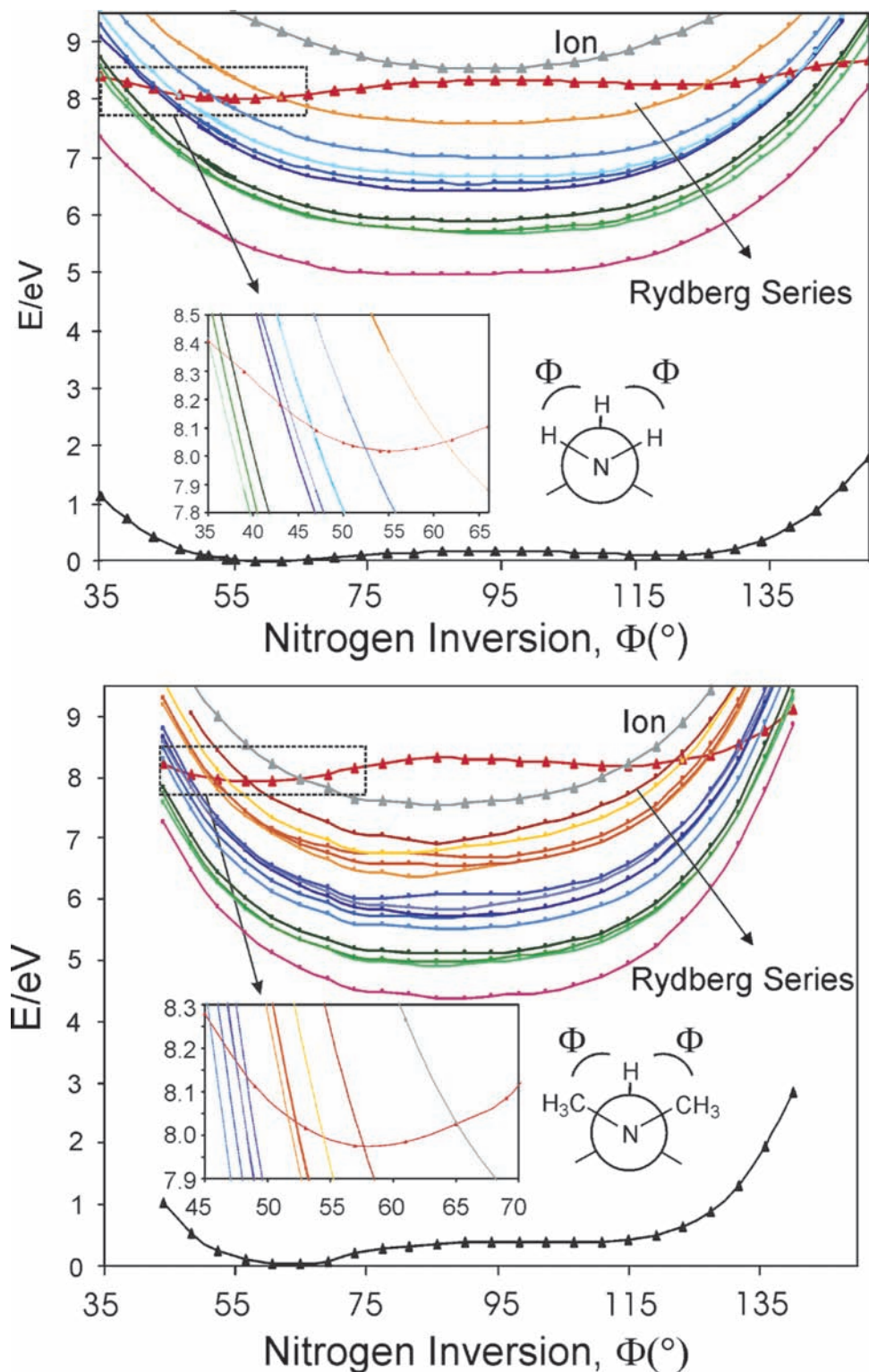


Figure 9. Scan of the potential energy surface for 2P and DM2P along the nitrogen inversion coordinate (ϕ) (TD-B3LYP/6-31++G(2df)//B3LYP/6-31+G(d)). The enlarged part shows the curve crossings between the $\sigma \rightarrow 3s$ state and the $n \rightarrow 3s, 3p, 3d,$ and $3f$ states, indicating the possible existence of conical intersections. Note the similarity in energetics between the scan for the primary and the tertiary amines. The purple curve corresponds to the $n \rightarrow 3s$ state whereas the green, blue, and yellow shaded curves correspond to the $n \rightarrow 3p, n \rightarrow 3d,$ and $n \rightarrow 3f$ states, respectively. The gray curve corresponds to the ground state of the ionized amine.

we find that there is a single 3s Rydberg state, three 3p Rydberg states, and five 3d Rydberg states.

Geometries. To establish which coordinate will take the initially formed wave packet out of the Franck–Condon (FC) region, the equilibrium geometry of the $n \rightarrow 3s$ excited species was calculated. Gradients have yet to be developed for TD-DFT approaches so this type of calculations does not provide a

viable strategy. We therefore employed CAS(4,3)/6-31+G(d) calculations and solved for the second root of the CI equations. Convergence problems for larger active spaces limited the exploration of the higher excited states. An alternative program package (MOLPRO 2000) showed a more smooth behavior. However, it is not possible to calculate vibrational frequencies under symmetry constraints and lowering the symmetry to C_1

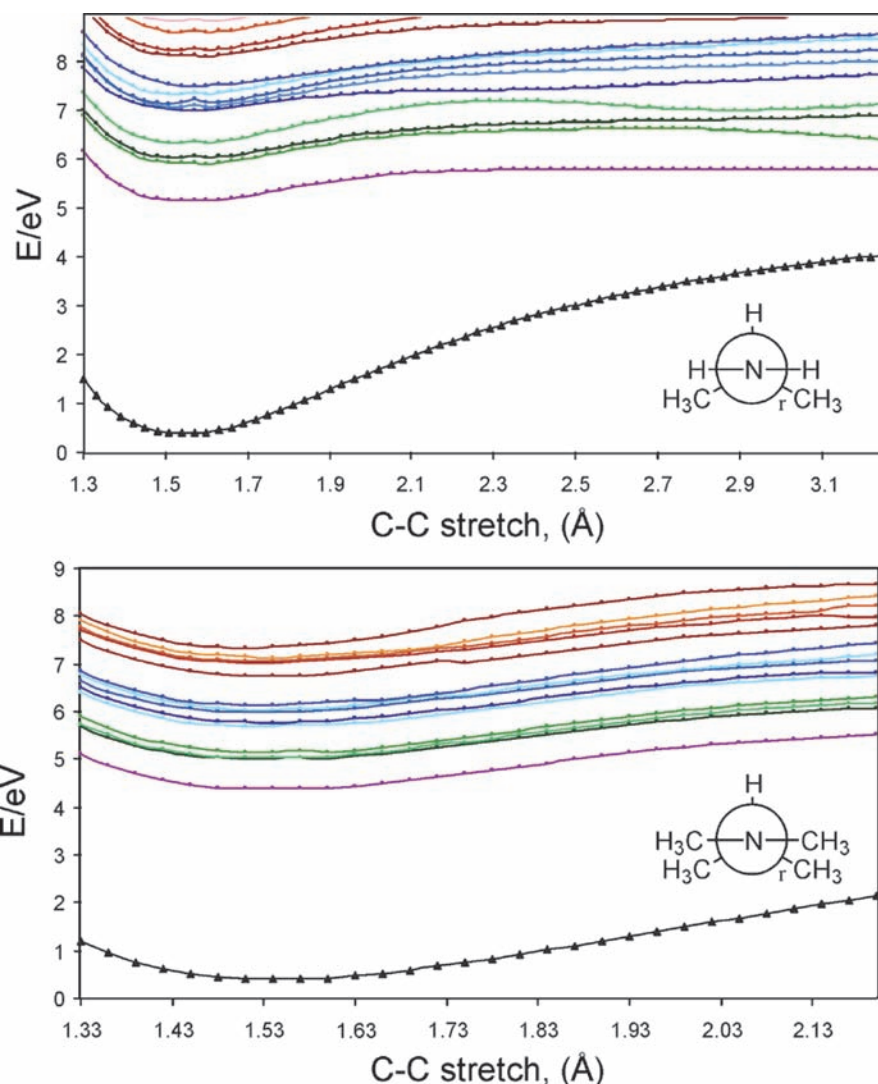


Figure 10. Scan of the potential energy surface for 2P and DM2P along the C–C bond breaking coordinate. The geometries were calculated for the ionized amine at the UB3LYP/6-31G(d) level, which means that the configuration around the nitrogen is planar during the C–C stretch ($\Phi = 90^\circ$ in Figure 9). The excited-state energies were calculated at the TD-B3LYP/6-31+G(d) level. Note the asymptotic behavior toward excited-state amino alkyl radicals.

reintroduced the convergence problems so this package was not employed any further.

The results for the equilibrium structure on the ground state and at $S_1(n \rightarrow 3s)$ surfaces are shown in Chart 2. Our computational results show that the energy change induced by rotation of the HNH plane is negligible and that the minimum-energy species has a HNH dihedral angle of either 0° or 90° depending on the state. The principal motion that takes the excited-state species out of the Franck–Condon region is therefore the planarization around the nitrogen atom. The appearance of the potential energy surface along this coordinate was therefore explored further and the results are presented in the following section.

Potential Energy Surface—The Nitrogen Inversion Coordinate. The calculated changes in energy with the symmetrical distortion of the HNCH dihedral angles (one for each hydrogen attached to the nitrogen atom) are shown in Figure 9 for 2P and (CNCH dihedrals) for DM2P. It can be seen from the figure that the appearance of the potential energy surface along ϕ is qualitatively very similar for 2P and DM2P. The only notable difference is that the potential energy difference between the Franck–Condon species and the equilibrium configuration of the excited-state species is larger in the case of the dimethylated

amine (~ 0.7 eV compared to ~ 0.5 eV for the primary amine). In both cases internal conversion between the Rydberg states is possible via a $\sigma \rightarrow 3s$ state that crosses with the Rydberg states. Such crossings may result in conical intersections that often are considered to give rise to “instantaneous” surface transitions.³² The result that the crossing features are so similar for the primary and the tertiary amines is consistent with the conclusion that the picosecond component of the dimethylated amines does not arise from an internal conversion process; if that was the case, one would not have expected the effect of dimethylation to be so large given the similarity of the calculated potential energy surfaces.

It is evident from Figure 9 and from the comparison of the calculated geometry at the equilibrium region of the excited state with the Franck–Condon geometry that the internal conversion from the initial highly excited Rydberg state can proceed via the nitrogen inversion coordinate. It would indeed seem plausible that this mode is the initially activated one and that it is therefore central for processes that occur on the femtosecond time scale. As the wave packet evolves along the $\sigma \rightarrow 3s$ state, the various crossing points are reached. At each crossing point the wave packet bifurcates; a fraction of it proceeds on the $\sigma \rightarrow 3s$ state (toward the remaining crossing

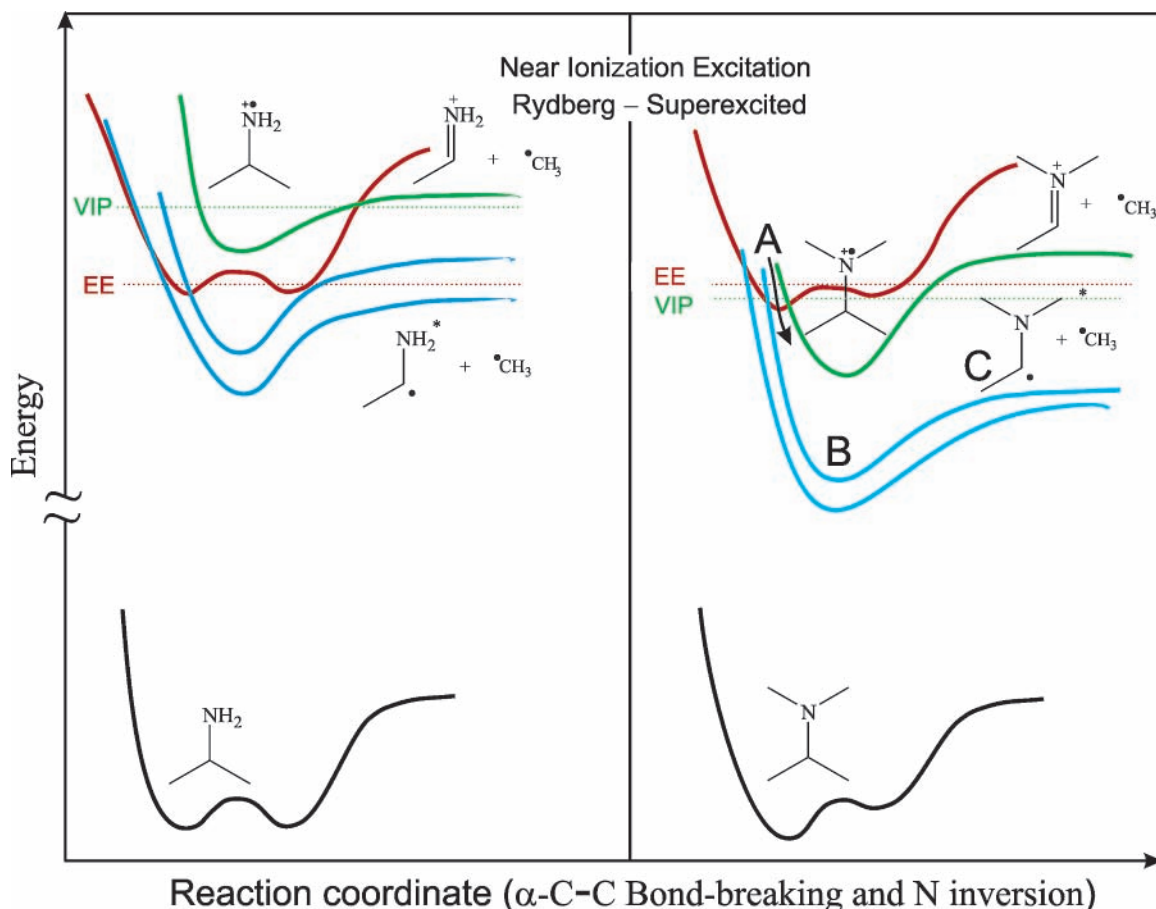
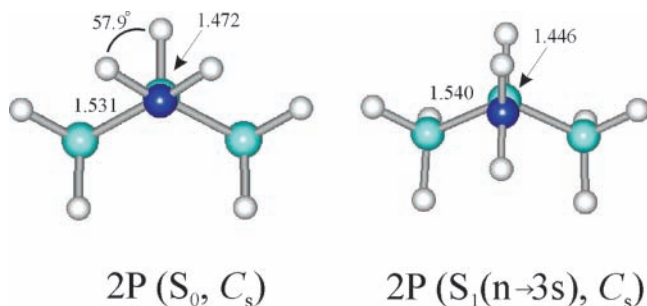


Figure 11. Generalized picture for the chemical and physical processes in primary and tertiary amines, excited near ionization.

CHART 2: Calculated Geometries (CAS(4,3)/6-31+G(d)) of the Equilibrium Structure on the Ground State and on the $S_1(n \rightarrow 3s)$ State

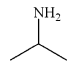
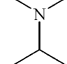


points), and a fraction ends up in a lower energy Rydberg state. The wave packet population becomes progressively more depopulated as the crossing points are passed along the $\sigma \rightarrow 3s$ state. As a consequence, it is primarily the first few Rydberg states below the initial state that are populated.

The energy change along other molecular degrees of freedom has also been calculated. The results show that internal conversion also in these cases can proceed via a $\sigma \rightarrow 3s$ state. However, the crossing points generally lie higher in energy compared to the PES cuts along the nitrogen inversion mode. Because of this and because the transition from the Franck-Condon region primarily involves the nitrogen inversion mode, the results are not discussed any further.

Potential Energy Surface—The C—C Bond Cleavage. To address the feasibility of a photochemically induced C—C bond breakage in amines, we have explored the potential energy surface along the α -C—C coordinate. The result is shown in

TABLE 4: Reaction Energies for Decomposition of Isopropylamine and *N,N*-Dimethylisopropylamine on Rydberg Surfaces^a

State of product amino alkyl radical		
$A''(\text{SOMO} \rightarrow 3s)$	5.16	4.98
$A''(\text{SOMO} \rightarrow 3p_z)$	5.83	5.57
$A''(\text{SOMO} \rightarrow 3p_y)$	5.94	5.67
$A'(\text{SOMO} \rightarrow 3p_x)$	6.58	5.98
$A''(\text{SOMO} \rightarrow 3d_{yz})$	6.85	6.22
$A''(\text{SOMO} \rightarrow 3d_z^2)$	7.16	6.31
$A''(\text{SOMO} \rightarrow 3d_{xz})$	7.67	6.57
$A'(\text{SOMO} \rightarrow 3d_x^2 - y^2)$	7.97	6.63
$A'(\text{SOMO} \rightarrow 3d_{xy})$	8.39	6.97
$A''(\text{SOMO} \rightarrow \text{Rydberg})^b$	8.48	7.34
$A''(\text{SOMO} \rightarrow \text{Rydberg})^b$	8.62	7.42
$A''(\text{SOMO} \rightarrow \text{Rydberg})^b$	9.14	7.76

^a TD-B3LYP/6-31++G(2df), values in eV, based on B3LYP/6-31++G(2df) cation geometries. ^b The angular momentum corresponding to the involved Rydberg orbital is unclear.

Figure 10 for the same manifold of Rydberg states as in the scans along the nitrogen inversion mode. The $\sigma \rightarrow 3s$ state (not shown) has an equilibrium C—C distance of around 1.80 Å. The potential energy associated with this state increases rapidly as the C—C bond is stretched further; this indicates that the products from bond breakage on this surface lie high in energy.

Structure and Reactivity

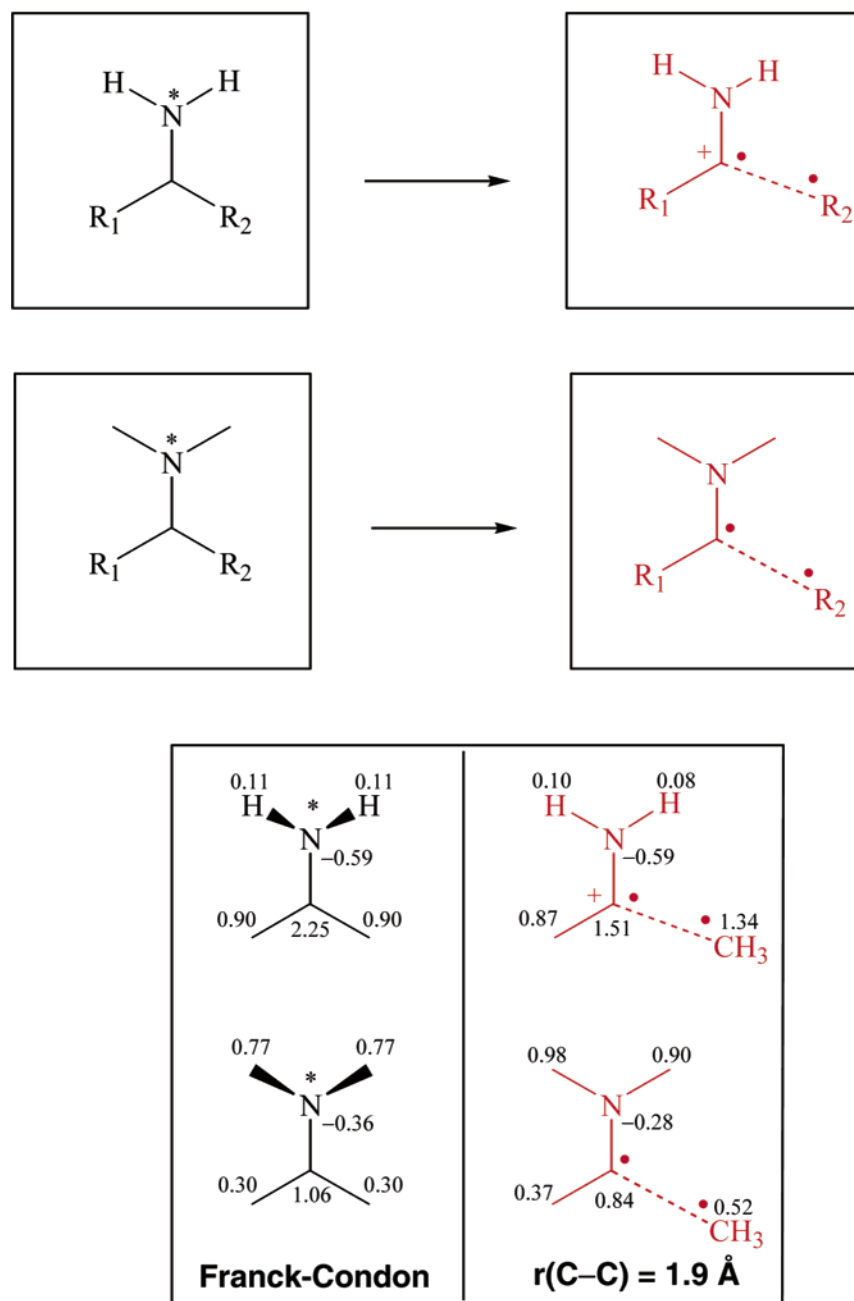


Figure 12. Correlation of structure and reactivity. The *N*-methyl substitution results in a smearing of charges and stabilizes the Rydberg states, leading to reactivity, not present in the unsubstituted amine. This idea is verified by a CIS/6-31++G(2df,p)/B3LYP/6-31G(d) calculation of the charges for $n \rightarrow 3d$ excited 2P and DM2P; the charges are shown in the bottom half of the figure for Franck-Condon excited species and for species where the C-C bond is partially broken.

For the Rydberg states, the potential energy approaches the combined potential energy of an excited-state product, aminoalkyl radical and a ground-state alkyl radical, as the C-C bond is stretched. The reaction energies for the formation of the 12 lowest lying excited-state aminoalkyl radicals and a ground-state methyl radical from 2P and DM2P are shown in Table 4. These values reflect the feasibility of the reaction under the assumption that an additional energy barrier does not exist. The TD-DFT scans seem to indicate that this is indeed the case. The most apparent trend that appears upon the comparison of the results for the primary and the tertiary amine is that the reaction energies are significantly smaller in the tertiary case.

In fact, for DM2P, it would seem to be energetically feasible at the available internal energy of 8.1 eV to break a C-C bond even on the highest lying Rydberg states depicted in Figure 10. The Rydberg-excited product resembles an ion, and that this is why the products become more stabilized upon alkyl substitution at the nitrogen. It is interesting to note that the C-C bond breakage is exothermic with respect to the Franck-Condon excited species (compare Tables 3 and 4).

Concluding General Picture of the Dynamics

The striking results presented here confirm the behavior of two classes of amines, differing in their substitution. For the

tertiary amines, the experimental (and theoretical) results support the decomposition of the excited amines via α -C–C bond breakage. The primary amine, however, does not undergo decomposition on the time scale of our experiments. Figure 11 shows a schematic presentation of how the potential energy changes for the near-ionization states when an unsubstituted or a substituted amine undergoes α -C–C bond breakage. A process that necessarily precedes the reactive pathway is the nonreactive internal conversion from a near-ionization state to the lower lying one(s).

For both the $-\text{NH}_2$ and the $-\text{N}(\text{CH}_3)_2$ systems, the wave packet proceeds in the direction that leads toward the equilibrium region of the near-ionization state in question. This was shown, by our calculations, to involve the nitrogen inversion mode and is basically a consequence of the near-ionization state being a bound Rydberg state—a cationic core separated from the valence electron. As the wave packet moves, it bifurcates to the lower lying Rydberg states ($A \rightarrow B$ in Figure 11). The periods of such inversion motions are known from IR-spectroscopy to range between 25 and 50 fs, so the motion out of the Franck–Condon region and down to the lower lying state is reflected in the value of τ_0 (50–170 fs) and in the transients taken at both the parent and the fragment masses because of decomposition of the parent ion.

In the case of the $-\text{N}(\text{CH}_3)_2$ amines, the α -C–C bond breakage is energetically feasible on the states that lie immediately below the initial Rydberg state. Because these states do not mix with lower lying states, the products are excited-state aminoalkyl radicals ($B \rightarrow C$, Figure 11). For the $-\text{NH}_2$ amines it is the low-lying states that are reactive; these will be populated only to a minor extent because the corresponding potential energy surfaces cross the $\sigma \rightarrow 3s$ state late on the nitrogen inversion coordinate. Thus, in this case, only the nonreactive internal conversion pathway is observed in the transients. It is a precursor for the ensuing bond breakage, which takes place in the $-\text{N}(\text{CH}_3)_2$ amines as it is possible to populate the reactive surface.

The picosecond component corresponds to α -C–C bond breakage; it materializes when the reaction is energetically allowed, i.e., for the $-\text{N}(\text{CH}_3)_2$ amines. This explains the observed dramatic substituent effect, which determines the relative contribution of the reactive and nonreactive channels, i.e., the shift of the picosecond to the femtosecond component. The control by IVR and the extent of redistribution could be verified in a deuterium labeling experiment. Because the primary amines do not decompose, one might have anticipated an offset at positive times in the corresponding transients. The fact that it is not always observed can be understood in terms of the 6 eV state that can be pumped by three 2 eV photons (negative times; i.e., the 615 nm pulses act as pump). This would give rise to an apparent depletion of the signal at either the parent or the fragment masses or at both (i.e., an apparent reduction of the signal intensity at positive times). The two effects work in opposite directions and cancel to a different extent, depending on the experimental conditions.

The reason for the difference in energetics for the α -C–C bond breakage in the $-\text{NH}_2$ and the $-\text{N}(\text{CH}_3)_2$ amines is the charged nature of the Rydberg states. Methyl group substitution on the nitrogen smears the positive charge on the cationic core and this results in a lowering of the energy of the Rydberg states, viewed along the reaction coordinate. This is not the case for the $-\text{NH}_2$ amines. In consequence, the reactive molecules will follow more ionic trajectories and the energy will in turn be higher. This idea is shown schematically in Figure 12.

An amine is generally viewed as substituted ammonia. The excited states of ammonia have been subjected to a variety of investigations, both experimentally and theoretically. For example, in a computational study, the ammonia spectrum was found to consist purely of Rydberg states with excitation energies higher than those of amines.³³ It has been shown that the lifetimes of amine Rydberg states can be on the femtosecond and picosecond time scale depending on whether the accessed state is reactive and on the accessed vibrational level.^{34,35} A mechanism similar to that of the dimethylated amines has been argued to be in play for hydrogen loss from ammonia excited to the \tilde{B} state;^{35a} a nonreactive internal conversion leads to the reactive $\tilde{A}A_2''$ state via the degenerate N–H stretch. The results for ammonia are in line with the femtosecond internal conversion mechanism that we discussed for the amines; the longer progression of the ammonia vibrational levels, compared to the larger and more complex amines, enables the study of a population of a specific vibrational level in the ammonia case.

The reaction times for the bond breaking processes are on the picosecond time scale. This contrasts the results for C–C bond breakage in ketones where the reaction occurs on the subpicosecond time scale. The reason for this difference is that during the internal conversion of a highly excited ketone the internal energy is funneled into the reactive mode through a conical intersection, during the initiating nonreactive internal conversion. This is not the case for the amines and the time scale for the reaction is, therefore, controlled by IVR or by the extent of redistribution. The discrepancy illustrates the importance of conical intersections for efficient reactivity in organic molecules.

Acknowledgment. This work was supported by the U.S. Office of Naval Research and the U.S. Air Force Office of Scientific Research. C.K., a Feodor Lynen Fellow from the Alexander von Humboldt Foundation, acknowledges the foundation and Caltech for support. T.I.S. was supported by Statens Naturvidenskabelige Forskningsraad, the Denmark-America foundation, and by Caltech, and thanks Dr. Steen Hammerum, University of Copenhagen, for valuable discussions.

References and Notes

- (1) (a) Platzman, R. L. *Vortex* **1962**, *23*, 372. (b) Platzman, R. L. *Radiation Res.* **1962**, *16*, 419. (c) Platzman, R. L. *J. Chem. Phys.* **1963**, *38*, 2775.
- (2) De Heer, F. J. *Int. J. Radiat. Phys. Chem.* **1975**, *7*, 137.
- (3) (a) Diau, E. W.-G.; Kötting, C.; Zewail, A. H. *ChemPhysChem* **2001**, *2*, 294. (b) Diau, E. W.-G.; Kötting, C.; Zewail, A. H. *ChemPhysChem* **2001**, *2*, 273. (c) Diau, E. W.-G.; Kötting, C.; Sølling, T. I.; Zewail, A. H. *ChemPhysChem* **2002**, *3*, 57. (d) Sølling, T. I.; Diau, E. W.-G.; Kötting, C.; De Feyter, S.; Zewail, A. H. *ChemPhysChem* **2002**, *3*, 79.
- (4) Kim, S. K.; Zewail, A. H. *Chem. Phys. Lett.* **1996**, *250*, 279.
- (5) (a) Kötting, C.; Diau, E. W. G.; Sølling, T. I.; Zewail, A. H. *J. Phys. Chem. A* **2002**, *106*, 7530. (b) Kötting, C.; Diau, E. W.-G.; Baldwin, J. E.; Zewail, A. H. *J. Phys. Chem. A* **2001**, *105*, 1677. (c) Gou, H.; Zewail, A. H. *Can. J. Chem.* **1994**, *72*, 947. (d) Janssen, M. H. M.; Dantus, M.; Guo, H.; Zewail, A. H. *Chem. Phys. Lett.* **1993**, *214*, 281.
- (6) Zewail, A. H. *Angew. Chem., Int. Ed.* **2000**, *39*, 2587.
- (7) (a) Zhong, D. P.; Cheng, P. Y.; Zewail, A. H. *J. Chem. Phys.* **1996**, *105*, 7864. (b) Dantus, M.; Janssen, M. H. M.; Zewail, A. H. *Chem. Phys. Lett.* **1991**, *181*, 281.
- (8) (a) Schick, C. P.; Weber, P. M. *J. Phys. Chem. A* **2001**, *105*, 3725. (b) Cheng, W.; Evans, C. L.; Kuthirummal, N.; Weber, P. M. *Chem. Phys. Lett.* **2001**, *349*, 2001.
- (9) See, for example; (a) Pinnaduwa, L. A.; Zhu, Y. *J. Chem. Phys.* **1998**, *108*, 6633. (b) Pinnaduwa, L. A.; Zhu, Y. *Chem. Phys. Lett.* **1997**, *277*, 147. (c) de Lange, C. A. *J. Chem. Soc., Faraday Trans.* **1998**, *94*, 3409. (d) Pan, C.-C.; Chou, C.-C.; Lu, C.-H.; Tai, Y.; Lin, K.-C. *J. Chem. Phys.* **1997**, *107*, 3797. (e) Ukai, M.; Kameta, K.; Machida, S.; Kouchi, N.; Hatano, Y.; Tanaka, K. *J. Chem. Phys.* **1994**, *101*, 5473.
- (10) Pinnaduwa, L. A.; Christophorou, L. G.; Bitouni, A. P. *J. Chem. Phys.* **1991**, *95*, 274.

- (11) (a) Noyes, W. A., Jr. In *Photochemistry and Reaction Kinetics*; Cambridge University Press: Cambridge, 1967 (see also references therein). (b) *Organic Photochemistry and Photobiology*; Horspool, W. M., Song, P.-S., Eds.; CRC Press: New York, 1995.
- (12) Hammerum, S.; Derrick, P. J. *J. Chem. Soc., Chem. Commun.* **1985**, 14, 996.
- (13) Hammerum, S.; Christensen, J. B.; Egsgaard, H.; Larsen, E.; Derrick, P. J.; Donchi, K. F. *Int. J. Mass Spectrom. Ion Phys.* **1983**, 47, 351.
- (14) Hammerum, S.; Norrman, K.; Sølling, T. I.; Andersen, P. E.; Jensen, L. B.; Vulpius, T. *J. Am. Chem. Soc.* Submitted.
- (15) Parker, D. H.; Bernstein, R. B.; Lichtin, D. A. *J. Chem. Phys.* **1981**, 75, 2577.
- (16) Herzberg, G.; Kolsch, R. Z. *Electrochem.* **1933**, 39, 572.
- (17) Von Sonntag, C.; Schuchmann, H. P. *Adv. Photochem.* **1977**, 10, 59.
- (18) Halpern, A. M. *Chem. Amino, Nitroso Nitro Compd. Their Deriv.* **1982**, 1, 155.
- (19) Taylor, D. P.; Bernstein, E. R. *J. Chem. Phys.* **1995**, 103, 10453.
- (20) Taylor, D. P.; Dion, C. F.; Bernstein, E. R. *J. Chem. Phys.* **1997**, 106, 3512.
- (21) Moritz, F.; Grotemeyer, J. *Org. Mass Spectrom.* **1993**, 28, 207.
- (22) Zewail, A. H. *Femtochemistry: Ultrafast Dynamics of the Chemical Bond*; World Scientific: Singapore, 1994 (see also references therein).
- (23) Kim, S. K.; Pedersen, S.; Zewail, A. H. *J. Chem. Phys.* **1995**, 103, 477.
- (24) Diau, E. W.-G.; De Feyter, S.; Zewail, A. H. *J. Chem. Phys.* **1999**, 110, 9785.
- (25) Scott, A. P.; Radom L. *J. Phys. Chem.* **1996**, 100, 16502.
- (26) Frisch, M. J.; Trucks, G. W.; Schlegel, H. B.; Scuseria, G. E.; Robb, M. A.; Cheeseman, J. R.; Zakrzewski, V. G.; Montgomery, J. A., Jr.; Stratmann, R. E.; Burant, J. C.; Dapprich, S.; Millam, J. M.; Daniels, A. D.; Kudin, K. N.; Strain, M. C.; Farkas, O.; Tomasi, J.; Barone, V.; Cossi, M.; Cammi, R.; Mennucci, B.; Pomelli, C.; Adamo, C.; Clifford, S.; Ochterski, J.; Petersson, G. A.; Ayala, P. Y.; Cui, Q.; Morokuma, K.; Malick, D. K.; Rabuck, A. D.; Raghavachari, K.; Foresman, J. B.; Cioslowski, J.; Ortiz, J. V.; Stefanov, B. B.; Liu, G.; Liashenko, A.; Piskorz, P.; Komaromi, I.; Gomperts, R.; Martin, R. L.; Fox, D. J.; Keith, T.; Al-Laham, M. A.; Peng, C. Y.; Nanayakkara, A.; Gonzalez, C.; Challacombe, M.; Gill, P. M. W.; Johnson, B. G.; Chen, W.; Wong, M. W.; Andres, J. L.; Head-Gordon, M.; Replogle, E. S.; Pople, J. A. *Gaussian 98*, rev. A.9; Gaussian, Inc.: Pittsburgh, PA, 1998.
- (27) Hunter, E. P.; Lias, S. G. *NIST Standard Reference Database Number 69, November 1998*; Mallard, W. G., Linstrom, P. J., Eds.; National Institute of Standards and Technology: Gaithersburg, MD (<http://webbook.nist.gov>).
- (28) (a) King, A. B. *J. Chem. Phys.* **1965**, 42, 3526. (b) Marshall, J. T. B.; Williams, D. H. *Tetrahedron.* **1967**, 23, 321. (c) Carpenter, W.; Duffield, A. M.; Djerassi, C. *J. Am. Chem. Soc.* **1967**, 89, 6167. (d) Brandt, R.; Djerassi, C. *Helv. Chim. Acta* **1968**, 51, 1750. (e) Brown, C. A.; Duffield, A. M.; Djerassi, C. *Org. Mass Spectrom.* **1969**, 2, 625.
- (29) Gandri, S. R.; Bernstein, R. B. *Chem. Phys.* **1986**, 105, 423.
- (30) Steinfeld, J. I.; Francisco, J. S.; Hase, W. L. *Chemical Kinetics and Dynamics*, 2nd ed.; Prentice Hall: Upper Saddle River, NJ, 1999.
- (31) Pedersen, S.; Zewail, A. H. *Mol. Phys.* **1996**, 89, 1455.
- (32) Robb, M. A.; Garavelli, M.; Olivucci, M.; Bernardi, F. In *Reviews in Computational Chemistry*; Lipkowitz, K. B., Boyd, D. B., Eds.; Wiley-VCH: New York, 2000; Vol. 15, pp 87–146.
- (33) Rianda, R.; Frueholz, R. P.; Goddard, W. A. *Chem. Phys.* **1977**, 19, 131.
- (34) (a) Baronavski, A. P.; Owrutsky, J. C. *J. Phys. Chem.* **1995**, 99, 10077. (b) Ritze, H.-H.; Radloff, I. V.; Hertel, I. V. *Chem. Phys. Lett.* **1998**, 289, 46. (c) Yin, S. H.; Liu, H. P.; Zhang, J. Y.; Jiang, B.; Xu, D. L.; Wang, L.; Sha, G. H.; Lou, N. Q. *Chem. Phys. Lett.* **2002**, 356, 227.
- (35) (a) Biesner, J.; Schnieder, L.; Schmeer, G.; Ahlers, G.; Xie, X.; Welge, K. H.; Ashfold, M. N. R.; Dixon, R. N. *J. Chem. Phys.* **1988**, 88, 3607. (b) Ashfold, M. N. R.; Dixon, R. N.; Little, N.; Stickland, R. J.; Western, C. M. *J. Chem. Phys.* **1988**, 89, 1754. (c) Dixon, R. N. *Chem. Phys. Lett.* **1988**, 147, 377. (d) Biesner, J.; Schnieder, L.; Ahlers, G.; Xie, X.; Welge, K. H.; Ashfold, M. N. R.; Dixon, R. N. *J. Chem. Phys.* **1989**, 91, 2901.